Noise-derived broadband full Green functions for a radially layered Earth

Lei LI
Email: ll.ynyf@gmail.com
Université Grenoble Alpes, CNRS, IRD, IFSTTAR, ISTerre, Grenoble, France

Abstract. The emerging noise correlation technique provides a way to approximate the Green function of medium with the correlation function between ambient noise wavefields. It has been recognized that not only the regularly observable seismic phase, but also spurious phases that have no correspondence in real seismograms, are constructed from noise correlations. In this study, we synthesize global noise correlations by stacking the source-wise correlation functions of numerically simulated Green functions for a spherically layered reference Earth model. The inelasticity and discontinuities of the Earth model are well honored. The synthetic data are broadband (3 to 300 s periods; from microseisms to seismic hum) and comprise the full components of the complete empirical Green functions that include all wave types. Comparisons between the results at periods of microseisms and seismic hum reveal that the noise-derived spurious phases should be primarily observable in the microseism period band, so do the core-related reflections and transmissions. Compared to real observations, S-type waves are supposed to be over-estimated in the secondary microseism frequency band. The data are publicly accessible from online repository (https://doi.org/10.6084/m9.figshare.8982506) and are promised to serve as reference to real-data noise correlations. The authors expect that the database of reference noise correlations can benefit the research of colleagues from the seismological or the whole solid-Earth community.

1 Introduction

Exploring Earth's inner structure is one of the fundamental tasks of geophysics. A common and efficient way is to extract information about the subsurface from the observations of seismic signals that pass through the medium. In the past, seismic applications had been primarily dependent on the energetic natural and artificial sources, like earthquakes and explosions. With the introduction of the correlation technique, or seismic interferometry, into the solid Earth seismology (Campillo & Paul 2003, Shapiro & Campillo 2004, Shapiro *et al.* 2005, Sabra *et al.* 2005, Yao *et al.* 2006), seismologists hold a tool to turn seismic noise into signals. By correlating long-time ambient noise records at two points, the Correlation Function (CF) is expected to approximate the Green Function (GF) of the medium between these two points, that is, the impulsive response recorded at one point when there is a source exciting at the other point. In some literatures (e.g., Yang & Ritzwoller 2008, Yao *et al.* 2009, Feng *et al.* 2017), the Ambient Noise Correlation (ANC) is also referred to as the Empirical Green Function (EGF), to be distinguished from the true GF. Nowadays, noise-based seismic imaging and monitoring have become routine geophysical methods and been widely applied at various scales from local to global.

It is indubitable that the one-dimensional reference Earth models, including PREM (Dziewonski & Anderson 1981), IASP91 (Kennett & Engdahl 1991) and AK135 (Kennett *et al.* 1995), have played very important roles in the advances of solid Earth seismology. The traveltimes and waveforms of seismic phases modelled from these models are broadly used for event location and phase identifications in real seismograms. Also, they are frequently used as initial or reference models in seismic imaging. As for ANCs, it has been known that the noise-derived seismic wavefields, or noise correlation wavefields, contain not only the regular seismic phases that have correspondence in real seismograms, but also spurious phases that do not obey the theory of seismic wave propagation (e.g., Boué *et al.* 2014, Li *et al.* 2019). The seismic wavefields directly simulated from the

reference models are not perfect reference to the noise correlation wavefields. It would be valuable to have an EGF database that can perform a better role of reference to real-data ANCs. Some authors have constructed global sections of CFs from synthetic or observed seismograms. Ruigrok et al. (2008) are pioneers in this aspect. They proposed a theory based on the acoustic correlation-type reciprocity theorem, and accordingly, simulated the global noise correlation wavefields from directly simulated seismic wavefields for a simplified PREM model that was acoustic, lossless, and without discontinuities above the transition zone. In their results, surface multiple reflections were extremely strong due to the lack of attenuation. Some spurious phases were observed, but simply ascribed to insufficient source sampling and numerical errors. One reason might be that the acoustic finite-difference code they used for seismic wavefield simulation were valid for rectangle grids that could not fit well to the Earth's geometry. The key reason could be that there were no global sections of real-data ANCs available for comparisons. Until five years later, Nishida (2013) constructed first the global sections of the vertical-vertical, radial-radial, transverse-transverse (or ZZ, RR and TT) components of real-data ANCs at periods of seismic hum from 25 s to 200 s (see their fig. 3), using nine years' continuous seismograms recorded by 658 worldwide broadband stations. The real-data sections contain several branches of body waves and surface waves, that are comparable to the corresponding theoretical GFs predicted by the normal mode theory. Haned *et al.* (2016) correlated the vertical components of two years' seismic hum data recorded by 149 global stations, at periods from 30 s to 250 s. They aimed toward inverting a global tomographic model of the upper mantle from the noise-derived Rayleigh waves, as Nishida *et al.* (2009) did. However, they showed the full waveforms of their ANCs, with both surface waves and body waves visible (see their fig. 4). It is an incomplete global ZZ section of hum correlations with inter-receiver distances ranging from 5º to 116º. Boué *et al.* (2013) calculated the CFs between the vertical components of continuous seismograms recorded by 339 global stations in one year. Their fig. 1 shows the ZZ section of global CFs filtered between 25 s and 100 s, in comparisons with the theoretical GFs modelled using the spectral element code AxiSEM (Nissen-Meyer *et al.* 2014) and the PREM model. Boué *et al.* (2013) used the least data but their results contain many more seismic phases than those of Nishida (2013) and Haned *et al.* (2016). It can be ascribed to that they used different datasets and data processing strategies. Haned *et al.* (2016) did not adopt traditional noise processing techniques (Bensen *et al.* 2007), but preferred a method of phase correlation followed by phase-weighted stack as proposed by Schimmel *et al.* (2011). Nishida (2013) adopted rigorous criteria to select the segments containing pure ambient noise from continuous seismograms. In contrast, Boué *et al.* (2013) retained the coda waves of global earthquakes in the computation of CFs. The resultant CFs include both ANCs and coda correlations. Based on the strength of daily CFs, Boué *et al.* (2014) divided the CF section in fig. 1(c) of Boué *et al.* (2013) into the so-called LCD and HCD sections (see their figs 4a and 4b). The LCD section is approximate to the ANCs, and the HCD section is closer to the coda correlations. Note that the coda wavefield excited by large earthquakes is essentially distinct from the ambient noise wavefield. The latter is dominated by ballistic seismic waves emanating from spatially distributed random noise sources, particularly, the seismic excitations induced by global ocean activities (Longuet-Higgins 1950, Hasselmann 1963, Hillers *et al.* 2012, Traer *et al.* 2012, Nishida 2014, Ardhuin *et al.* 2015, Tanimoto *et al.* 2015, Deen *et al.* 2018, Gualtieri *et al.* 2019). In contrast, the coda wavefields are dominated by high-order free oscillations at longer periods, due to their low attenuations (Maeda *et al.* 2006, Poli *et al.* 2017). Consequently, the coda correlations are distinct from the ANCs. The differences can be observed directly by comparing the ZZ section of global coda correlations in fig. 2 of Phạm *et al.* (2018) with the ZZ sections of global noise correlations in fig. 3(a) of Nishida (2013), fig. 4(a) of Boué *et al.* (2014) and fig. 4 of Haned *et al.* (2016). The noise correlation wavefield mimics the theoretical seismic wavefield, whereas the coda correlation wavefield appears quite different from the theoretical one. The coda correlation wavefield contains excessively energetic core-related phases and an abundant amount of strong spurious phases.

The global real-data ANC sections introduced above are hum correlations at periods longer than 25 s. Currently, a global section of real-data microseism correlations, to our knowledge, is still missing. The CFs computed by Boué *et al.* (2013) are for periods from 1 s to 100, but the low coherence of noise-derived signals for station pairs at varying geographical locations

impeded the construction of a high-fidelity global section. Some authors presented sections of ANCs for specific seismic networks within limited distance ranges (e.g., fig. 2c of Boué *et al.* 2014, fig. 1b of Feng *et al.* 2017, fig. 2 of Spica *et al.* 2017, fig. 4 of Li *et al.* 2019). The synthetic results by Ruigrok et al. (2008) are the only global sections available at periods of microseisms (their figs 10 and 11). However, the results are based on an over-simplified model. To sum up, a reference database for global ANCs is still missing. In this paper, we synthesize an elaborate database of all the components of the EGFs, for the reference AK135 Earth model with density and Q values from Montagner & Kennett (1996), namely, the so-called AK135f model. The database is publicly accessible and we expect it can facilitate the noise-based studies and applications [see Campillo & Roux (2015) for a review]. The paper is organized as follows. First, we revisit the theoretical formulae to synthesize the EGFs. Then, we describe the technical details on the synthetization of the EGFs from directly simulated seismograms. After, we present the results of all the nontrivial components of the EGFs, and compare them with the numerically simulated theoretical GFs and with existing real-data correlations published in previous studies. Also, we discuss causes for the potential discrepancies between the synthetic and real-data EGFs.

2 Theory

The ambient seismic wavefield can be deemed as a superposition of random waves from spatially distributed noise sources (Aki 1965, Cox 1973), namely,

$$X(f) = \sum_i S_i(f) G(s_i, r; f), \qquad (1)$$

where *f*, *S* and *G* are seismic frequency, source process and GF, respectively; *s* and *r* represent source and receiver, respectively; subscript *i* denotes the indices of noise sources. Theories have proved that the time derivative of the CF between ambient wavefields at two points *A* and *B*, converges toward the GF of medium between these two points (e.g., Roux et al., 2005; Weaver and Lobkis, 2001). In real practices, it is common to approximate GF with CF itself, namely,

$$G_{AB} \sim C_{AB}, \qquad (2)$$

to avoid extra errors introduced by differentiation (Roux *et al.* 2005).

Assuming uncorrelated noise sources, the correlations between waves from different sources trend to vanish at a long time. Thereby, the CF between *A* and *B* can be computed from a summation of the CFs for independent sources:

$$C_{AB}(f) = X_A(f) X_B^*(f) = \sum_i |S_i(f)|^2 G(s_i, r_A; f)\, G^*(s_i, r_B; f). \qquad (3)$$

$|S_i(f)|^2$ is the power spectra of noise source, so the equation can be deemed as a source power weighted stack of the CFs between the source-receiver GFs. In an ideal case of uniform source distribution, the source power term is a constant and can be omitted. The stack of the source-wise CFs is also referred to by authors as source averaging (e.g., Larose et al., 2006) or integral (e.g., Ruigrok et al., 2008). Here, we prefer to mention it as source stack due to the discrete, summation form of Eq. (3).

3 Methods

Equation (3) indicates that inter-receiver ANCs can be synthesized from source-receiver GFs, with additional knowledge of source power spectra (Woodard 1997). As for the Earth planet, seismic noise sources are primarily distributed on or close to the surface (Ardhuin *et al.* 2015, Tanimoto *et al.* 2015, Nishida 2017). Thus, we consider a two-dimensional model with discrete point sources equally spaced on the global surface (Fig. 1a). Regarding the GFs for the reference Earth model, we use AxiSEM to simulate the seismograms for a point force source and equally-spaced receivers all at surface. The synthetic seismograms are the strict GFs (response to an input Dirac pulse) convolved with a Gaussian source wavelet used in the simulation. Here we simply refer to them as GFs. Providing single force sources in Z, R and T directions, all the components of the GF tensor can be obtained: Z and R seismograms for a vertical force correspond to the ZZ and ZR components of GFs;

Z and R seismograms for a radial force correspond to the RZ and RR components of GFs; T seismograms for a transverse force correspond to the TT components of GFs. The remaining components of GFs are expected to be trivial for a radially layered Earth and are thus omitted. From the directly simulated GFs (Fig. 1b), one can see that except the surface waves, few seismic phases are prominent after two hours. Thus, we compute the CFs using two-hour-long seismograms. The maximum lag of the CFs is constrained by the length of the correlated seismograms. The amplitude of CF decays apparently when the lag approaches the seismogram length and vanishes when the lag is longer than the seismogram length.

In real practices, it is common to normalize CF with the power of the correlated noise records, namely,

$$\tilde{C}_{AB} = \frac{C_{AB}}{|X_A||X_B|}. \qquad (4)$$

The tilde bar stands for normalization. For uniform source distribution, the denominator in Eq. (4) is invariant for any pair of stations on Earth's surface. It appears convenient to synthesize the reference EGFs for evenly distributed sources using Eq. (4). However, in that case, seismic energy from distant sources that experiences more reflections/transmissions, absorptions and spreading, will be dwarfed by the excessive energy from sources close to the station (see the variations of seismic energy with source-receiver distance from Fig. 1c). It implies that the results of Eq. (4) will be heavily dominated by sources close to stations, and of course, the resulting EGFs will resemble the theoretical GFs. It has been known that the most energetic noise sources are oceanic (e.g., Longuet-Higgins 1950, Peterson 1993, Ardhuin *et al.* 2015, Nishida 2017), while the most majority of seismic stations are deployed on land. Also, the global oceanic noise sources can never be uniform but vary largely in space and time (see e.g., Landés *et al.* 2010, Hillers *et al.* 2012). Generally, we can hardly expect strong noise sources collocated with stations. To suppress the dominance of the nearby sources in the source stack, one may simply choose to discard them, as done by Ruigrok *et al.* (2008). However, it is a problem to set a reasonable threshold to the source-receiver distances. Recall that our aim is to provide reference EGFs for real-data ANCs. We expect there can be more seismic phases that are clear in the synthetic correlation wavefields, no matter it is a physical or spurious one. Thus, we do not prefer a uniform source distribution, but modify Eq. (3) to meet our needs:

$$\tilde{C}_{AB}(f) = \sum_i \tilde{G}(s_i, r_A; f)\, \tilde{G}^*(s_i, r_B; f). \qquad (5)$$

The GFs at any source-receiver distances are normalized by their own norms, so that any source can play a relatively balanced role in the source stack. One can also choose to process the GFs with the time-domain equalization techniques that are routinely used in noise data processing (e.g., Bensen *et al.* 2007). However, these techniques, such as one-bit sampling and running absolution mean, are non-linear and heavily change the waveforms. The normalization in Eq. (5) is linear and retains the shape of waveforms and the relative strength of seismic phases.

We summarize the procedures of the EGF simulation as follows. The nontrivial components (ZZ, ZR, RZ, RR, TT) of two-hour-long theoretical GFs are synthesized using the AxiSEM code. The GFs are bandpass filtered between 3 s and 300 s. Based on Eq. (5), global ANCs are synthesized from the filtered GFs.

Figure 1(d) illustrates the synthetization of the inter-receiver ANC for a pair of stations 68º apart, through the source stack by Eq. (5). The acausal part of the CF at negative time delays corresponds to the waves propagating from receiver A to receiver B, while the causal part at positive time delays corresponds to the waves from B to A. All the sources on the major arc between A and B can contribute to the construction of the surface wave traveling between A and B along the minor arc. Sources on the minor arc between A and B lead to the construction of the surface wave between A and B along the major arc, which is outside the time axis of the panel. The surface waves in the directly simulated seismograms are much stronger than body waves. Consequently, they still dominant in the CFs. From the rightmost panel, one can see that body waves are also well constructed. Figure 1(e) displays an enlarged part of Figure 1(d). The left panel shows the waveform stacked for distances from 105º to 165º. This range includes the stationary-phase source location for the causal P wave, which is 134º to receiver A and 68º to

receiver B, but exclude the stationary-phase location for the PP wave, which is 102º to receiver A and 34º to receiver B. However, part of the Fresnel zone for the PP wave is included in this range. The stack over the source-wise CFs is still constructive, leading to a visible PP signal. Similarly, despite there is no stationary point on the curve of time delays between P and PKPab waves, the source stack can be constructive to produce a spurious signal at between 7 and 8 minutes. Li *et al.* (2019) studied this spurious phase specifically. The authors observed strong signals caused by the PKPab-P correlations, from the real-data ANCs between seismic stations deployed in Japan and Finland, respectively. This mechanism was proposed to term as quasi-stationary phase condition, to be discriminated from the strict stationary phase condition.

4 Results and discussions

The synthetic global ANC database is online accessible from data repository at https://doi.org/10.6084/m9.figshare.8982506. The ZZ, RR and TT components are time-symmetric and thus only the causal parts of CFs are stored. The ZR and RZ components are fully stored. Other components are assumed to be zeros. The data are stored in mat format that are easy to handle in Matlab or Python. Sample codes to read and plot the data are available from the repository.

Figure 2 displays the global sections of the envelopes of the synthetic EGFs, in the period band of microseisms (5 to 25 s) and in comparisons with the theoretical GFs. Theoretical traveltime curves of some seismic phases, calculated using the Taup program (Crotwell *et al.* 1999), are provided in Fig. 2(f) to aid locating these phases. One can observe from Fig. 2 that a majority of the seismic phases are well reconstructed from the correlations. Also, there are many branches of spurious phases that have no correspondence in the theoretical GFs. Li *et al.* (2019) proposed a double-array method to unveil the ray paths of the interfering waves that generate a particular seismic signal, by estimating the traveltime delay and the respective slownesses of the interfering waves. They applied the method to a spurious phase observed from real-data ANCs between Japan and Finland seismic arrays. The method is also applicable to the analysis of the correlation-derived phases in Fig. 2.

In spite of lacking a global section of real-data microseism correlations for comparisons, we anticipate some discrepancies between the synthetic data and real observations. One major difference would be regarding the energy partition between wave types. The frequency-dependent excitation mechanisms and energy partition of seismic noise spectra among different wave types, is summarized by Nishida (2017) in their fig. 2. As for the most energetic secondary microseism, the dominant sources are the oceanic wave-wave interactions that are equivalent to vertical forces exerting to the ocean surface (Longuet-Higgins 1950, Hasselmann 1963). The S waves originate from the conversions of P waves at the ocean bottom (Gualtieri *et al.* 2014) and are much weaker than the P waves in the secondary microseisms. That has been confirmed by seismological observations (e.g., Nishida & Takagi 2016, Liu *et al.* 2016). In our modeling, the single force sources are placed on a solid crustal surface. Undoubtedly, the energy of microseism S waves in our simulation is over-estimated in comparisons to real observations. The sources are placed on the surface, and the one-dimensional reference Earth model has high Q values in the lithosphere. These factors lead to that surface waves are too strong in the global wavefields. In real world, many parts of the Earth's crust are highly attenuating and heterogeneous. Absorptions, lateral density/velocity gradients, steep interfaces and random scattering can significantly attenuate the surface waves and reduce their coherence. There have even been reports on stronger P waves than Rayleigh waves (e.g., Vinnik 1973, Koper *et al.* 2010). Overall, the surface waves and shear waves are over-estimated in the synthetic ANC data.

Figure 3 shows the synthetic ANCs and theoretical GFs in the period band of seismic hum (25 to 100 s). Comparing to Fig. 2, there are few spurious phases emerging in Fig. 3. The missing of spurious phases from CFs of seismic hum is consistent with the real-data observations by other authors (Nishida 2013, Boué *et al.* 2014, Haned *et al.* 2016). It implies that the spurious

phases are easier to be observed at the shorter periods of microseisms, and rarer at the longer periods of seismic hum. Another prominent feature is that in Fig. 3, core-related reflections and transmissions are weaker/fewer. Clear S waves and the surface multiples appear in the synthetic hum correlations. This is compatible with the real-data results (Nishida 2013, Boué *et al.* 2014, Haned *et al.* 2016). Nishida (2013) observed a strong *PL* phase following the direct P phase in the ZZ and RR components of hum correlations at separation distances less than 40º. The phase corresponds to a leaking spheroidal mode in the crust-mantle waveguide, Figure 3(f) shows the synthetic hum correlations in the same range as fig. 3(c) of Nishida (2013). There seems to be a faint *PL*-like phase in the ZZ components. But it should just be a visual illusion.

The synthetic ANC data are computed under ideal conditions, with signals been enhanced. It is natural to expect that not all the phases discernible in the synthetic data, either physical or spurious, would be constructed from real data, especially for those generated from the interference between faint phases. In real-data ANCs, sometimes conspicuous noise-derived signals can arise from very localized strong noise sources (e.g., Shapiro *et al.* 2006, Zeng & Ni 2010). These signals are not included in the synthetic ANC data. Last, we emphasize that the synthetic ANC database is planned for ambient noise that is dominated by ballistic waves, but not for the earthquake codas that are comprised of free oscillations.

5 Conclusions

In this study, we simulate the global ANCs by stacking the source-wise CFs of theoretical GFs for the AK135f model. Comparing to the simulation by Ruigrok *et al.* (2008) for an acoustic lossless PREM model without discontinuities in and above the upper mantle, we use the original AK135f model and thus our results include all types of waves (P, S and surface waves), with attenuation and interfaces of the model appropriately respected. Our results cover a broad band of 3 to 300 s and the full components of ANCs, which is another advantage over the previous studies. We share the data in a public online repository, prospecting that the data can serve as a good reference to real-data ANCs and accordingly facilitate the various noise-based studies and applications.

References

Aki, K. (1965) A note on the use of microseisms in determining the shallow structure of the Earth's crust. *Geophysics*, **30**, 665–666, Society of Exploration Geophysicists. doi:10.1190/1.1439640

Ardhuin, F., Gualtieri, L. & Stutzmann, E. (2015) How ocean waves rock the Earth: Two mechanisms explain microseisms with periods 3 to 300s. *Geophys. Res. Lett.*, **42**, 765–772. doi:10.1002/2014GL062782

Bensen, G.D., Ritzwoller, M.H., Barmin, M.P., Levshin, A.L., Lin, F., Moschetti, M.P., Shapiro, N.M., *et al.* (2007) Processing seismic ambient noise data to obtain reliable broad-band surface wave dispersion measurements. *Geophys. J. Int.*, **169**, 1239–1260. doi:10.1111/j.1365-246X.2007.03374.x

Boué, P., Poli, P., Campillo, M., Pedersen, H., Briand, X. & Roux, P. (2013) Teleseismic correlations of ambient seismic noise for deep global imaging of the Earth. *Geophys. J. Int.*, **194**, 844–848. doi:10.1093/gji/ggt160

Boué, P., Poli, P., Campillo, M. & Roux, P. (2014) Reverberations, coda waves and ambient noise: Correlations at the global scale and retrieval of the deep phases. *Earth Planet. Sci. Lett.*, **391**, 137–145. doi:10.1016/j.epsl.2014.01.047

Campillo, M. & Paul, A. (2003) Long-Range Correlations in the Diffuse Seismic Coda. *Science (80-.).*, **299**, 547–549. doi:10.1126/science.1078551

Campillo, M. & Roux, P. (2015) Crust and Lithospheric Structure - Seismic Imaging and Monitoring with Ambient Noise Correlations. in *Treatise on Geophysics*, pp. 391–417. doi:10.1016/B978-0-444-53802-4.00024-5

Cox, H. (1973) Spatial correlation in arbitrary noise fields with application to ambient sea noise. *J. Acoust. Soc. Am.*, **54**, 1289–1301, Acoustical Society of America. doi:10.1121/1.1914426

Crotwell, H.P., Owens, T.J. & Ritsema, J. (1999) The TauP Toolkit: Flexible Seismic Travel-time and Ray-path Utilities. *Seismol. Res. Lett.*, **70**, 154–160. doi:10.1785/gssrl.70.2.154

Deen, M., Stutzmann, E. & Ardhuin, F. (2018) The Earth's hum variations from a global model and seismic recordings around the Indian Ocean. *Geochemistry, Geophys. Geosystems*, Wiley-Blackwell. doi:10.1029/2018GC007478

Dziewonski, A.M. & Anderson, D.L. (1981) Preliminary reference Earth model. *Phys. Earth Planet. Inter.*, **25**, 297–356. doi:10.1016/0031-9201(81)90046-7

Feng, J., Yao, H., Poli, P., Fang, L., Wu, Y. & Zhang, P. (2017) Depth variations of 410 km and 660 km discontinuities in eastern North China Craton revealed by ambient noise interferometry. *Geophys. Res. Lett.*, **44**, 8328–8335. doi:10.1002/2017GL074263

Gualtieri, L., Stutzmann, E., Farra, V., Capdeville, Y., Schimmel, M., Ardhuin, F. & Morelli, A. (2014) Modelling the ocean site effect on seismic noise body waves. *Geophys. J. Int.*, **197**, 1096–1106. doi:10.1093/gji/ggu042

Gualtieri, L., Stutzmann, E., Juretzek, C., Hadziioannou, C. & Ardhuin, F. (2019) Global scale analysis and modeling of primary microseisms. *Geophys. J. Int.* doi:10.1093/gji/ggz161

Haned, A., Stutzmann, E., Schimmel, M., Kiselev, S., Davaille, A. & Yelles-Chaouche, A. (2016) Global tomography using seismic hum. *Geophys. J. Int.*, **204**, 1222–1236, Oxford University Press. doi:10.1093/gji/ggv516

Hasselmann, K. (1963) A statistical analysis of the generation of microseisms. *Rev. Geophys.*, **1**, 177–210. doi:10.1029/RG001i002p00177

Hillers, G., Graham, N., Campillo, M., Kedar, S., Landès, M. & Shapiro, N. (2012) Global oceanic microseism sources as seen by seismic arrays and predicted by wave action models. *Geochemistry, Geophys. Geosystems*, **13**, Q01021. doi:10.1029/2011GC003875

Kennett, B. & Engdahl, E.R. (1991) Traveltimes for global earthquake location and phase identification. *Geophys. J. Int.*, **105**, 429–465, Blackwell Publishing Ltd. doi:10.1111/j.1365-246X.1991.tb06724.x

Kennett, B.L.N., Engdahl, E.R. & Buland, R. (1995) Constraints on seismic velocities in the Earth from traveltimes. *Geophys. J. Int.*, **122**, 108–124. doi:10.1111/j.1365-246X.1995.tb03540.x

Koper, K.D., Seats, K. & Benz, H. (2010) On the composition of earth's short-period seismic noise field. *Bull. Seismol. Soc. Am.*, **100**, 606–617. doi:10.1785/0120090120

Landés, M., Hubans, F., Shapiro, N.M., Paul, A. & Campillo, M. (2010) Origin of deep ocean microseisms by using teleseismic body waves. *J. Geophys. Res. Solid Earth*, **115**, 1–14. doi:10.1029/2009JB006918

Larose, E., Margerin, L., Derode, A., Tiggelen, B. van, Campillo, M., Shapiro, N., Paul, A., *et al.* (2006) Correlation of random wavefields: An interdisciplinary review. *Geophysics*, **71**, SI11–SI21. doi:10.1190/1.2213356

Li, L., Boué, P. & Campillo, M. (2019) Observation and explanation of spurious seismic signals emerging in teleseismic noise correlations. *Solid Earth Discuss.*, 1–20, Copernicus GmbH. doi:10.5194/se-2019-118

Liu, Q., Koper, K.D., Burlacu, R., Ni, S., Wang, F., Zou, C., Wei, Y., *et al.* (2016) Source locations of teleseismic P, SV, and SH waves observed in microseisms recorded by a large aperture seismic array in China. *Earth Planet. Sci. Lett.*, **449**, 39–47. doi:10.1016/j.epsl.2016.05.035

Longuet-Higgins, M.S. (1950) A Theory of the Origin of Microseisms. *Philos. Trans. R. Soc. A Math. Phys. Eng. Sci.*, **243**, 1–35. doi:10.1098/rsta.1950.0012

Maeda, T., Sato, H. & Ohtake, M. (2006) Constituents of Vertical-component Coda Waves at Long Periods. *Pure Appl. Geophys.*, **163**, 549–566, Birkhäuser-Verlag. doi:10.1007/s00024-005-0031-9

Montagner, J.P. & Kennett, B.L.N. (1996) How to reconcile body-wave and normal-mode reference earth models. *Geophys. J. Int.*, **125**, 229–248. doi:10.1111/j.1365-246X.1996.tb06548.x

Nishida, K. (2013) Global propagation of body waves revealed by cross-correlation analysis of seismic hum. *Geophys. Res. Lett.*, **40**, 1691–1696. doi:10.1002/grl.50269

Nishida, Kiwamu. (2014) Source spectra of seismic hum. *Geophys. J. Int.*, **199**. doi:10.1093/gji/ggu272

Nishida, Kiwamu. (2017) Ambient seismic wave field. *Proc. Japan Acad. Ser. B*, **93**, 423–448, The Japan Academy. doi:10.2183/pjab.93.026

Nishida, Kiwamu, Montagner, J.-P.J.-P. & Kawakatsu, H. (2009) Global Surface Wave Tomography Using Seismic Hum. *Science (80-.).*, **326**, 112–112, American Association for the Advancement of Science. doi:10.1126/science.1176389

Nishida, Kiwamu & Takagi, R. (2016) Teleseismic S wave microseisms. *Science (80-.).*, **353**, 919–921. doi:10.1126/science.aaf7573

Nissen-Meyer, T., Driel, M. van, Stähler, S.C., Hosseini, K., Hempel, S., Auer, L., Colombi, A., *et al.* (2014) AxiSEM: broadband 3-D seismic wavefields in axisymmetric media. *Solid Earth*, **5**, 425–445. doi:10.5194/se-5-425-2014

Peterson, J. (1993) Observations and Modeling of Seismic Background Noise. *U.S. Geol. Surv. Open File Rep. 93-322*.

Phạm, T.-S., Tkalčić, H., Sambridge, M. & Kennett, B. (2018) Earth's Correlation Wavefield: Late Coda Correlation. *Geophys. Res. Lett.*, **45**, 3035–3042, Wiley-Blackwell. doi:10.1002/2018GL077244

Poli, P., Campillo, M. & Hoop, M. de. (2017) Analysis of intermediate period correlations of coda from deep earthquakes. *Earth Planet. Sci. Lett.*, **477**, 147–155. doi:10.1016/j.epsl.2017.08.026

Roux, P., Sabra, K.G., Kuperman, W.A. & Roux, A. (2005) Ambient noise cross correlation in free space: Theoretical approach. *J. Acoust. Soc. Am.*, **117**, 79–84, Acoustical Society of America. doi:10.1121/1.1830673

Ruigrok, E., Draganov, D. & Wapenaar, K. (2008) Global-scale seismic interferometry: Theory and numerical examples. *Geophys. Prospect.*, **56**, 395–417. doi:10.1111/j.1365-2478.2008.00697.x

Sabra, K.G., Gerstoft, P., Roux, P., Kuperman, W.A. & Fehler, M.C. (2005) Surface wave tomography from microseisms in Southern California. *Geophys. Res. Lett.*, **32**, 1–4. doi:10.1029/2005GL023155

Schimmel, M., Stutzmann, E. & Gallart, J. (2011) Using instantaneous phase coherence for signal extraction from ambient noise data at a local to a global scale. *Geophys. J. Int.*, **184**, 494–506, Wiley/Blackwell (10.1111). doi:10.1111/j.1365-246X.2010.04861.x

Shapiro, N. M. & Campillo, M. (2004) Emergence of broadband Rayleigh waves from correlations of the ambient seismic noise. *Geophys. Res. Lett.*, **31**, 8–11. doi:10.1029/2004GL019491

Shapiro, N. M., Ritzwoller, M.H. & Bensen, G.D. (2006) Source location of the 26 sec microseism from cross-correlations of ambient seismic noise. *Geophys. Res. Lett.*, **33**, L18310. doi:10.1029/2006GL027010

Shapiro, Nikolai M., Campillo, M., Stehly, L. & Ritzwoller, M.H. (2005) High-resolution surface-wave tomography from ambient seismic noise. *Science (80-.).*, **307**, 1615–1618. doi:10.1126/science.1108339

Spica, Z., Perton, M. & Beroza, G.C. (2017) Lateral heterogeneity imaged by small-aperture ScS retrieval from the ambient seismic field. *Geophys. Res. Lett.*, **44**, 8276–8284. doi:10.1002/2017GL073230

Tanimoto, T., Heki, K. & Artru-Lambin, J. (2015) Interaction of Solid Earth, Atmosphere, and Ionosphere. in *Treatise on Geophysics*, 2nd editio., Vol. 4, pp. 421–443, Elsevier. doi:10.1016/B978-044452748-6.00075-4

Traer, J., Gerstoft, P., Bromirski, P.D. & Shearer, P.M. (2012) Microseisms and hum from ocean surface gravity waves. *J. Geophys. Res.*, **117**, 1–16. doi:10.1029/2012JB009550

Vinnik, L.P. (1973) Sources of microseismicP waves. *Pure Appl. Geophys.*, **103**, 282–289, Birkhäuser-Verlag. doi:10.1007/BF00876404

Weaver, R.L. & Lobkis, O.I. (2001) Ultrasonics without a Source: Thermal Fluctuation Correlations at MHz Frequencies. *Phys. Rev. Lett.*, **87**, 134301. doi:10.1103/PhysRevLett.87.134301

Woodard, M.F. (1997) Implications of Localized, Acoustic Absorption for Heliotomographic Analysis of Sunspots. *Astrophys. J.*, **485**, 890–894, IOP Publishing. doi:10.1086/304468

Yang, Y. & Ritzwoller, M.H. (2008) Characteristics of ambient seismic noise as a source for surface wave tomography. *Geochemistry, Geophys. Geosystems*, **9**, n/a-n/a. doi:10.1029/2007GC001814

Yao, H., Campman, X., Hoop, M. V. de & Hilst, R.D. van der. (2009) Estimation of surface wave Green's functions from correlation of direct waves, coda waves, and ambient noise in SE Tibet. *Phys. Earth Planet. Inter.*, **177**, 1–11, Elsevier. doi:10.1016/j.pepi.2009.07.002

Yao, H., Hilst, R.D. van der & Hoop, M. V de. (2006) Surface-wave array tomography in SE Tibet from ambient seismic noise and two-station analysis - I. Phase velocity maps. *Geophys. J. Int.*, **166**, 732–744, Oxford University Press. doi:10.1111/j.1365-246X.2006.03028.x

Zeng, X. & Ni, S. (2010) A persistent localized microseismic source near the Kyushu Island, Japan. *Geophys. Res. Lett.*, **37**, L24307. doi:10.1029/2010GL045774

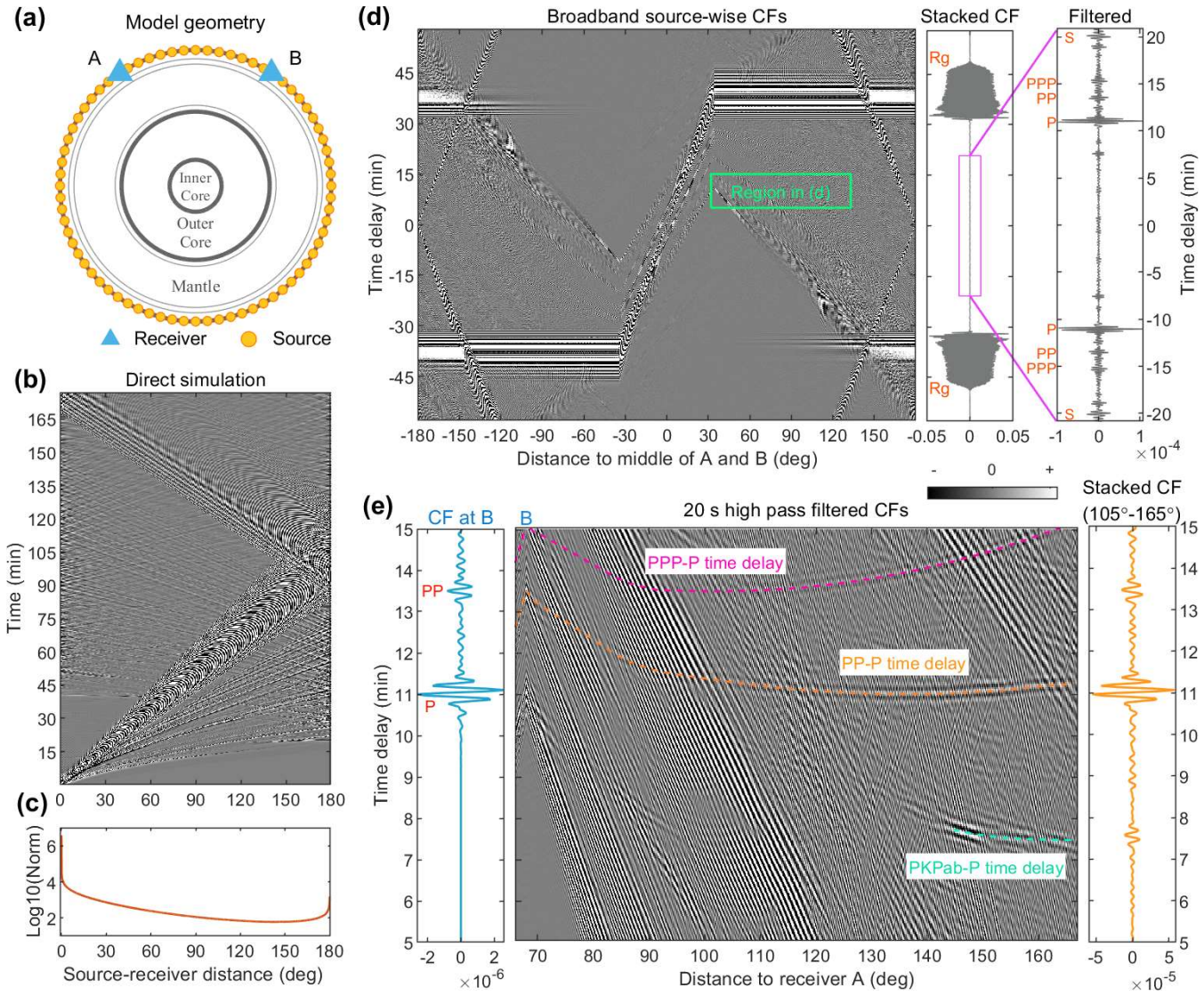

Figure 1: (a) Geometry of the model for synthesizing the inter-receiver ANC. (b) Global seismograms simulated using AxiSEM. (c) Variations of the logarithm of norms of two-hour seismograms with respect to distance. (d) Source stack for synthesizing the ANC between two stations 68° apart, at periods from 10 s to 100 s. (e) An enlarged part of (d), at periods from 10 s to 20 s.

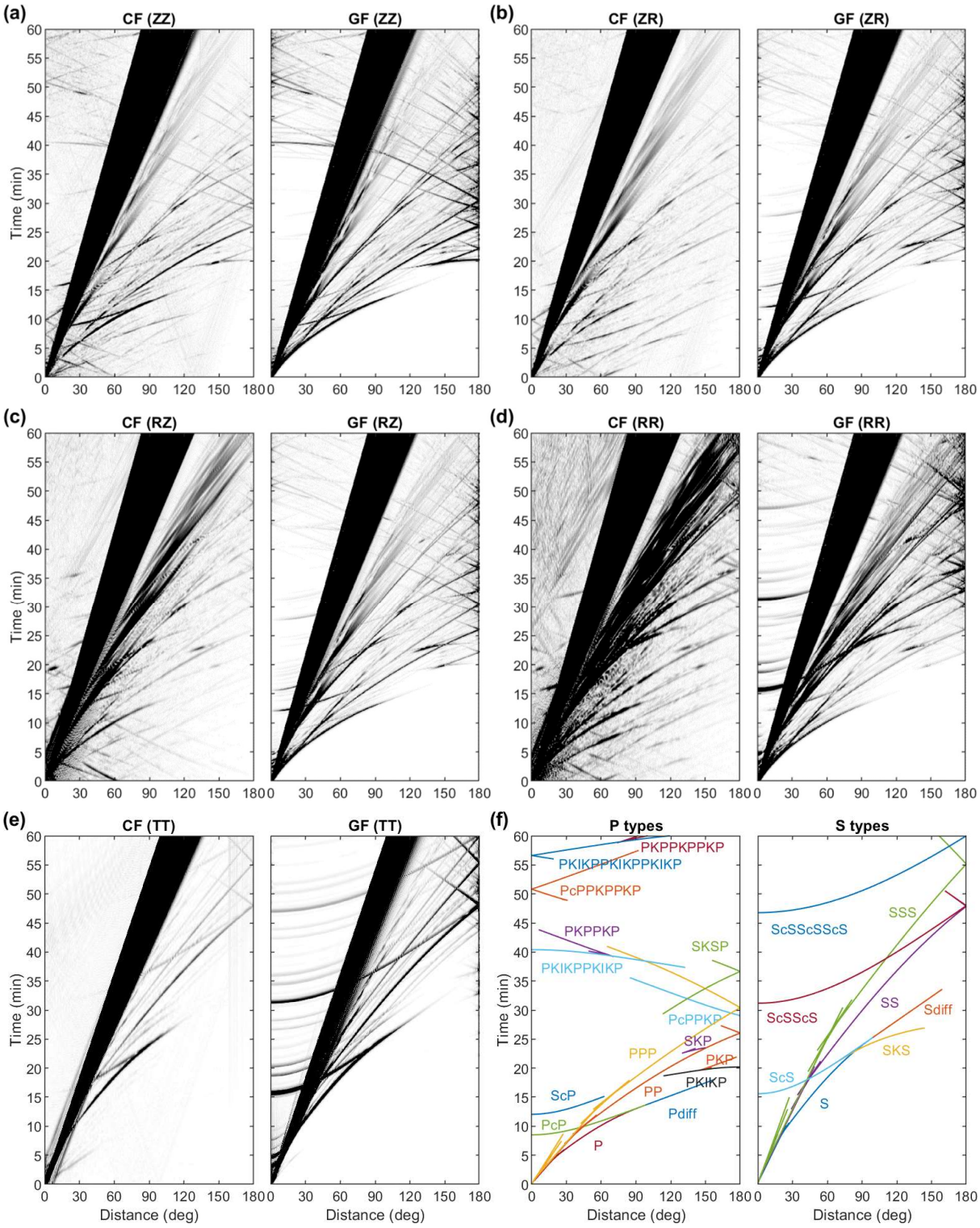

Figure 2: Global sections of synthetic EGFs in the period band of microseisms (3 to 20 s), in comparisons with theoretical GFs: (a) ZZ, (b) ZR, (c) RZ, (d) RR, (e) TT. (f) Theoretical traveltimes of seismic phases predicted by the Taup program.

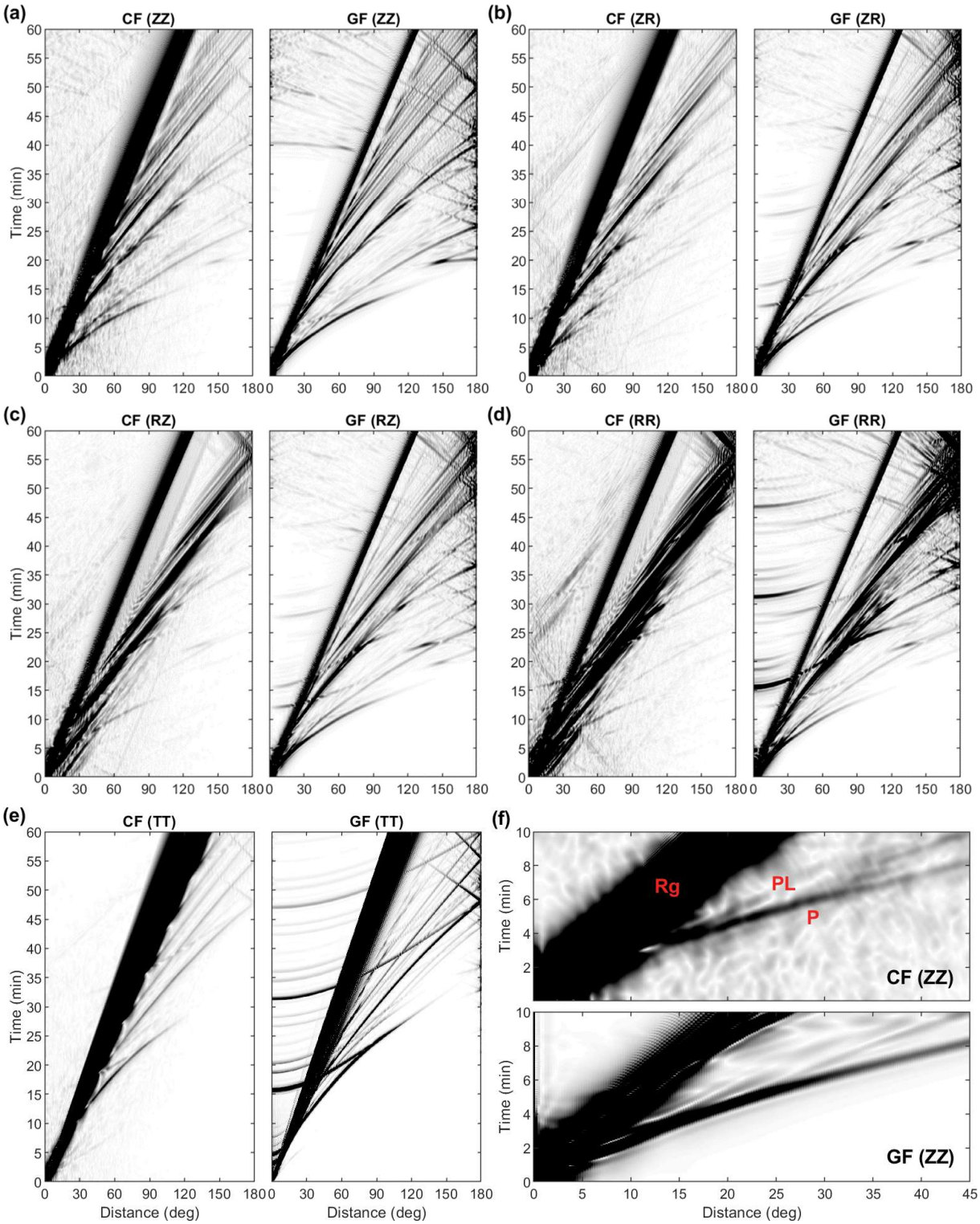

Figure 3: Global sections of synthetic EGFs in the period band of seismic hum (25 to 100 s), in comparisons with theoretical GFs: (a) ZZ, (b) ZR, (c) RZ, (d) RR, (e) TT. (f) Enlarge parts of ZZ and RR components of EGFs in (a).